CHEMISTRY OF MATERIALS

Article

pubs.acs.org/cm

Propagative Exfoliation of High Quality Graphene

Lan Feng,[†] Yue-Wen Liu,[†] Xing-Yan Tang,[†] Yanmei Piao,[‡] Shu-Fen Chen,[†] Shun-Liu Deng,*[,†] Su-Yuan Xie,[†] YuHuang Wang,*[,‡] and Lan-Sun Zheng[†]

[†]Department of Chemistry and State Key Laboratory of Physical Chemistry of Solid Surface, College of Chemistry and Chemical Engineering, Xiamen University, Xiamen 361005, China

[‡]Department of Chemistry and Biochemistry, University of Maryland, College Park, Maryland 20742, United States

Supporting Information

ABSTRACT: High quality graphene materials that readily disperse in water or organic solvents are needed to achieve some of the most ambitious applications. However, current synthetic approaches are typically limited by irreversible structural damages, little solubility, or low scalability. Here, we describe a fundamental study of graphene chemistry and covalent functionalization patterns on sp^2 carbon lattices, from which a facile, scalable synthesis of high quality graphene sheets was developed. Graphite materials were efficiently exfoliated by reductive, propagative alkylation. The exfoliated, propagatively alkylated graphene sheets (PAGenes) not only exhibited high solubility in common solvents such as chloroform, water, and *N*-methyl-pyrrolidone, but also showed electrical conductivity as high as 4.1×10^3 S/m, which is 5 orders of magnitude greater than those of graphene oxides. Bright blue photoluminescence, unattainable in graphene, was also observed. We attribute the rise of blue photoluminescence in PAGenes to small on-graphene sp^2 domains created by the propagative covalent chemistry, which may expand from graphene edges or existing defect sites leaving sp^2-hybridized patches interlaced with sp^3-hybridized regions. The intact sp^2 domains enable effective electrical percolation among different graphene layers affording the observed high electrical conductivity in PAGene films.

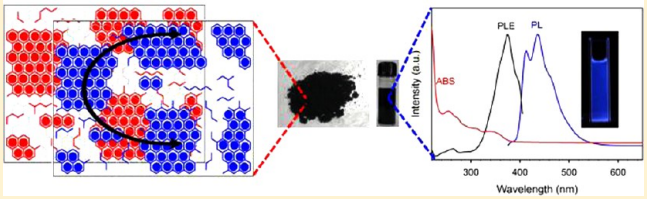

KEYWORDS: *graphitic materials, chemical functionalization, electrical percolation, photoluminescence, functionalization pattern, band gap engineering*

1. INTRODUCTION

Graphene has attracted enormous attention over the past few years due, in part, to the remarkable electrical, mechanical, and thermal properties of this new material.[1] Methods such as micromechanical cleavage,[2] epitaxial growth,[3] and chemical vapor deposition (CVD)[4−6] are successful in producing high quality materials that have fueled the fundamental research of graphene. However, low yield and throughput remain limiting factors for these methods in producing large quantities of materials needed for many practical applications, such as capacitors, fuel cells, catalysts, and sensors.[7−10] In addition, graphene materials produced by these methods typically have poor dispersibility, limiting their processing capabilities. Alternatively, graphene can be synthesized at low cost and large scale by extensive oxidation and subsequent exfoliation of graphite.[11,12] This method can be traced back to the early work of Hummers in the 1950s[13] and remains one of the most widely adapted synthetic methods for graphene materials. The produced graphene oxides (GOs) are chemically functionalized with oxygen-containing functional groups such as epoxides, carboxyl, and hydroxyl groups[14] such that they can be readily dispersed in water to form a homogeneous dispersion. However, GOs face several other challenging technical limitations. Particularly difficult are the electrically insulating nature of GOs and the irreversibility of the oxidation chemistry. Although most of the oxygen moieties could be removed by chemical reduction or by thermal treatment, the process leaves irreversible chemical damage as oxygen strips carbon off the graphene lattice.[11] Nonchemical methods such as direct exfoliation of pristine graphite using surfactants or organic solvents can also produce graphene layers in liquid media.[15] In comparison with GOs, this method circumvents the harsh oxidation chemistry and the destruction of carbon basal planes, affording less defective graphene layers. However, since graphite is insoluble, the direct exfoliation in solution phase usually involves lengthy processing time and extensive sonication, resulting in the creation of cracks and structural defects in graphene layers. Hence, a more feasible and reliable method for large-scale production of high quality graphene materials, dispersible in water or organic solvents, is still urgently needed.

Reductive activation followed by *in situ* covalent functionalization is an efficient route for the exfoliation and functionalization of carbon-based materials such as carbon nanotubes (CNTs) and graphene sheets.[16−19] Recently, we found that propagative sidewall alkylcarboxylation of CNTs by

Received: May 20, 2013
Revised: October 18, 2013
Published: October 21, 2013

   dx.doi.org/10.1021/cm402880v | *Chem. Mater.* 2013, 25, 4487−4496

the Billups–Birch reduction led to water-soluble functional structures with interesting optical and electrical properties.[20−25] CNT bundles were spontaneously exfoliated as they were charged by solvated electrons in liquid ammonia.[16,17] The Coulombic repulsions overcome the strong van der Waals interactions between CNTs. Addition of alkyl halide to the homogeneous dispersion resulted in efficient sidewall functionalization of CNTs. Moreover, we found that the alkylation occurred by defect activation propagating exclusively from sp^3 defect sites,[20] which makes it possible to control the spatial pattern of functional groups on sp^2 carbon lattices.

Here, we show that propagative alkylation of graphite leads to large-scale exfoliation and controlled functionalization of graphene sheets (Scheme 1). Both graphite and highly ordered

Scheme 1. Schematic Illustration of Exfoliation and Alkylation of Graphene Sheets

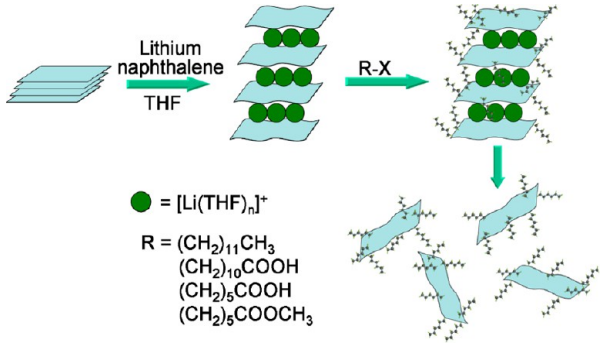

pyrolytic graphite (HOPG) were reduced by alkali metal in the presence of an aromatic hydrocarbon such as naphthalene in tetrahydrofuran (THF). Efficient exfoliation of graphene sheets occurs as the alkylation reaction gradually propagates from the graphite edges, producing exfoliated and propagatively alkylated graphene sheets (PAGenes). Unlike the graphene layers obtained by oxidation and mechanical exfoliation of graphite, PAGenes not only exhibit excellent dispersibility in organic solvents or water, depending on the terminating functional groups, but also show blue photoluminescence and high electrical conductivity. Structural evolution and characterizations of PAGenes suggest that the covalently functionalized structures develop an interesting pattern best described as sp^2 islands interlaced with sp^3 matrixes within the lattice of graphene. High conductivity thus became possible due to electrical percolation among graphene layers via contacts of nonfunctionalized regions.

2. EXPERIMENTAL SECTION

2.1. Materials. Graphite powder (<5 μm) was purchased from Nanjing XFNANO Materials Tech Co., Ltd. (Nanjing, China). Highly oriented pyrolytic graphite (HOPG) was acquired from Structure Probe, Inc. (SPI-2 grade). CoMoCat single-walled carbon nanotubes (SWCNTs) were purchased from SouthWest NanoTechnologies, Inc. 1-Bromododecane (98%) was purchased from Sinopharm Chemical Reagent Co. Ltd. (Shanghai, China). 6-Bromohexanoic acid (96%) was purchased from TCI (Shanghai, China). 11-Bromoundecanoic acid (97.5%) and methyl 6-bromohexanoate (98%) were purchased from Accela ChemBio Co., Ltd. (Shanghai, China). THF was purchased from Sinopharm Chemical Reagent Co. Ltd. (Shanghai, China) and was redistilled before use. Pentacene (98%), coronene (98%), and anthracene (99%) were purchased from J&K Scientific Co., Ltd. (Beijing, China). Other chemicals and solvents were commercially available and used as received.

2.2. Reductive Alkylation of Graphite. Under Ar protection, 55.8 mg of graphite (~4.65 mmol of carbon) was added to 150 mL of freshly distilled THF in a round-bottom flask, in which lithium (0.98 g, 142 mmol) and naphthalene (4.9 g, 38.3 mmol) had also been added. With the aid of stirring, the lithium gradually dissolved to give a dark green solution. After 35 min, 1-bromododecane was slowly added at a rate of 0.3 mL/min using an injection pump until the green color disappeared. The mixture was allowed to react for 12 h. After the reaction, 10 mL of ethanol was added to quench the unreacted lithium. Then, the solid products were collected by vacuum filtration. The products were repeatedly washed with toluene, ethanol, and water. The final solid, G-C_{12}_1, was dried in a vacuum oven at 60 °C for 12 h. The alkylation reactions were conducted for up to 8 cycles using a recycling procedure previously developed in our lab.[21] The obtained products were named with G-C_{12}_n, in which n indicates the number of reaction cycles.

When 1-bromododecane was replaced by other alkyl halide agents, such as 6-bromohexanoic acid, 11-bromoundecanoic acid, and methyl 6-bromohexanoate, alkylated products with different functional groups were obtained. The corresponding products were named G-C_5COOH_n, G-C_{10}COOH_n, and G-C_5COOCH_3_n, respectively. The reductive alkylation reactions were also performed on HOPG.

2.3. Thermal Defunctionalization of PAGenes. Thermal defunctionalization experiments were performed with a SDT Q600 thermogravimetric analysis (TGA) instrument. The samples were held at 80 °C for 30 min, with 100 sccm N_2 as the protecting and carrying gas, followed by temperature increase to 700 °C at a rate of 10 °C/min. The same thermal treatment was performed on pristine graphite as a control.

Thermal defunctionalization of PAGenes for electrical conductivity measurement was performed in a quartz tube furnace (Φ 42 mm × 600 mm) with 100 sccm H_2 and 280 sccm Ar. The temperature was held at 100 °C for 1 h, and then ramped to 550 °C at a rate of 5 °C/min. The samples were held at 550 °C for 1.5 h before cooling to room temperature.

2.4. Electrical Conductivity Measurement. The electrical conductivity of PAGenes films was measured on a microcontrolled probe station (D41-11A/ZM, JianZhong Machinery, Beijing) using a four probe method. PAGene powder was compressed into films using a FW-4 compression machine (Tianjin Sky Optical Instrument Co., Ltd.). Each PAGenes film was measured five times at different areas to ensure the uniformity of the conductivity. The corresponding conductivity (σ, S/m) was calculated using the formula $\sigma = 1/(R_s t)$, where R_s is the sheet resistance (unit: Ω/sq), and t is the film thickness (unit: m). The electrical conductivity of GOs was measured as a control in a similar way.

2.5. Characterization. *Powder X-ray Diffraction (XRD).* Powder X-ray diffraction (XRD) patterns were recorded on a Rigaku Ultima IV diffractionmeter with Cu Kα radiation (λ = 1.54 18 Å) and a graphite monochromator from 5° to 90° at a scanning rate of 10°/min.

Scanning Electron Microscopy (SEM) and Transmission Electron Microscopy (TEM). SEM images were obtained on a Hitachi S-4800 scanning electron microscope. For sample preparation, the as-prepared products were suspended in ethanol by brief sonication for 2–3 min, and then carefully deposited on a silicon wafer by drop casting. TEM images were obtained on a TECNAI F-30 transmission electron microscope. The ethanol solution of the as-prepared product was deposited on a lacey carbon coated, 300-mesh copper grid using a pipet.

Raman Spectroscopy. Raman spectra were obtained on a Renishaw Invia Raman microscope using a 532 nm excitation line. As-prepared PAGenes were suspended in ethanol by brief sonication in a bath sonicator, and the solution was deposited dropwise on a glass microscope slide and allowed to dry at room temperature. For each sample, spectra were measured at several separated spots and averaged. Raman mapping of the D-band (1246–1413 cm^{-1}) was recorded on a Horiba Jobin Yvon XploRa Raman microscope at a step size of 1 μm, using a 532 nm excitation line and a 100× objective.

Atomic Force Microscopy (AFM). AFM images were recorded on an Agilent 550 AFM instrument (Agilent Technologies) in tapping

dx.doi.org/10.1021/cm402880v | Chem. Mater. 2013, 25, 4487–4496

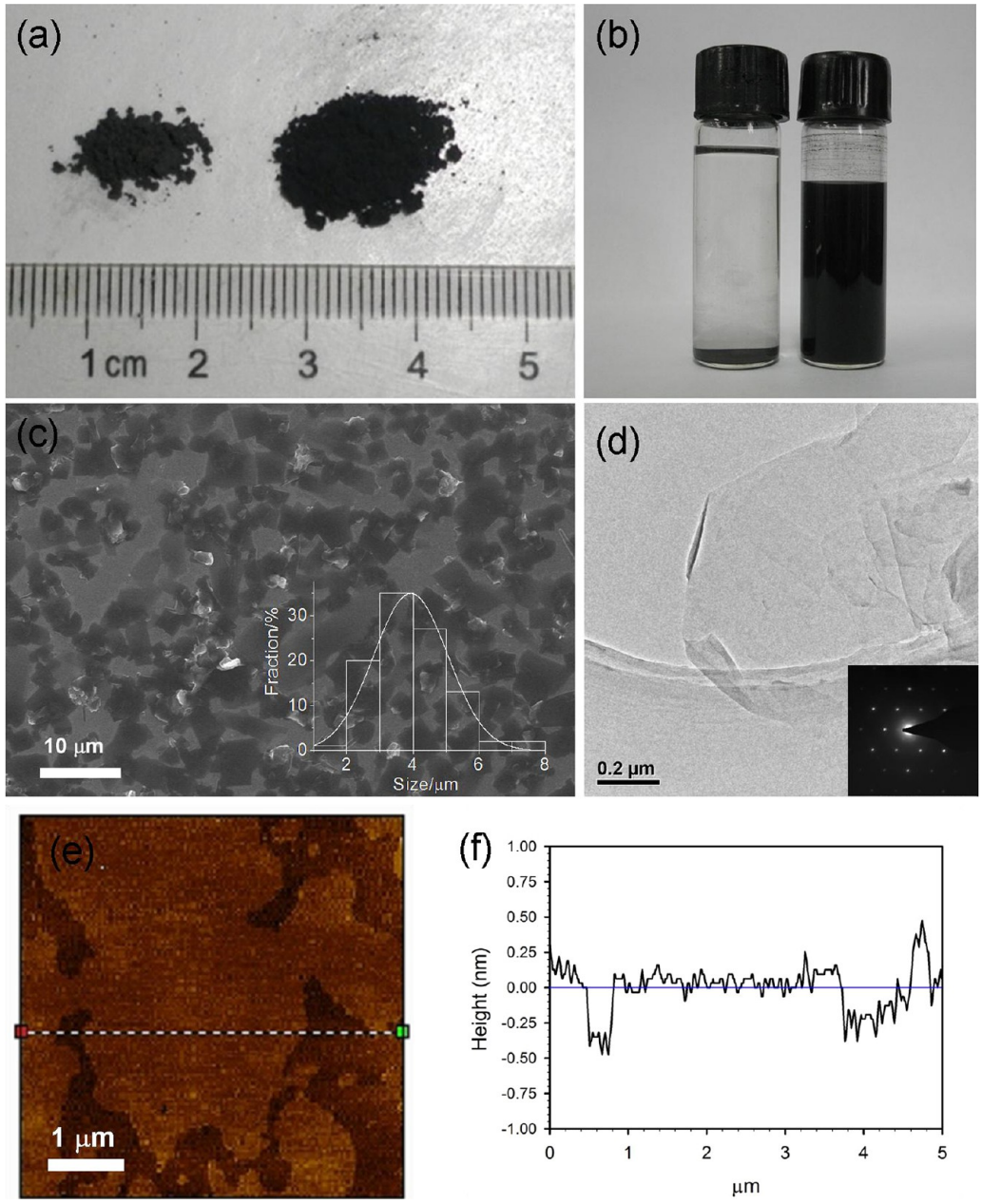

Figure 1. Dodecylated PAGenes. (a) PAGenes prepared by eight cycles of alkylation (G-C_{12}_8) (right) have a much larger volume compared with the same amount (10 mg) of pristine graphite (left). (b) The chloroform dispersions of G-C_{12}_8 (right) and pristine graphite (left). (c) SEM and (d) TEM images of the PAGenes. (e) AFM image of PAGenes with the corresponding height profile of a line scan (f). The insets in parts c and d show the lateral size distribution of PAGenes and the selected area electron diffraction pattern, respectively.

mode. Samples were prepared by dropping ethanol suspended PAGenes on a mica substrate.

UV–Vis Absorption Spectroscopy and Fluorescence Spectroscopy. Absorption spectra were recorded on a Shimadzu UV-2550 absorption spectrometer using 1 cm quartz cuvettes. Emission spectroscopy was performed on an F-7000 fluorescence spectrophotometer. PAGenes were suspended in ethanol by bath sonication for 5 min. After that, the solution was centrifuged on a SIGMA 3K15 refrigerated centrifuge at 9000 rpm for 5 min to obtain an isotropic supernatant. Since graphene dots with very small size (typically less than 10 nm) resulted from the reactions and damages of the original large graphene sheets can affect the absorption and emission spectroscopy of PAGenes, the obtained supernatant was discarded, and the sediment was redispersed in ethanol for the optical measurement.

For comparative spectroscopy studies with small aromatic compounds, anthracene, pentacene, and coronene were dissolved in cyclohexane, followed by centrifugation at 14 000 rpm for 10 min to obtain isotropic solutions for the optical measurement. The absorption and emission spectra were measured on Shimadzu UV-2550 absorption spectrometer and F-7000 fluorescence spectrophotometer, respectively.

IR Spectroscopy. Graphite and PAGenes were suspended in dichloromethane by sonication. Then, a drop of the dispersion was dried on the surface of a NaCl plate for IR measurement using a Nicolet 380 FT-IR spectrometer.

3. RESULTS AND DISCUSSION

3.1. Exfoliation of Graphite through Propagative Alkylation. Figure 1a shows dodecylated PAGenes prepared

dx.doi.org/10.1021/cm402880v | *Chem. Mater.* 2013, 25, 4487–4496

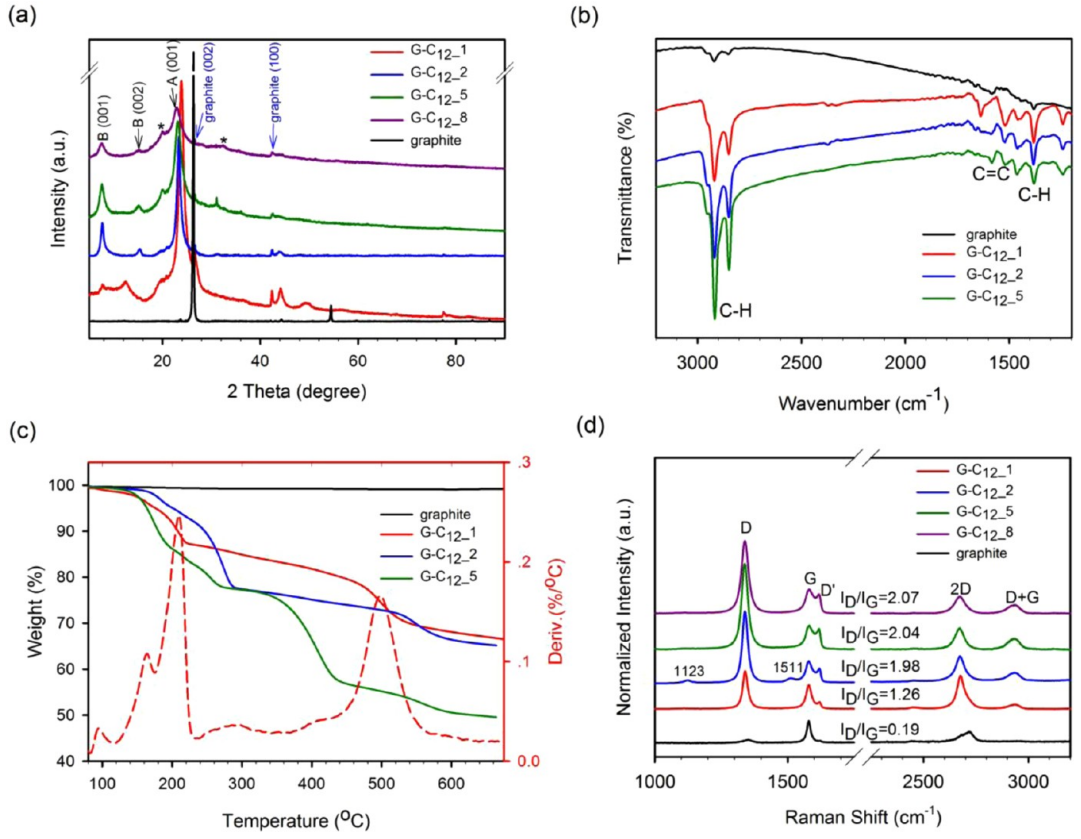

Figure 2. Structural evolution of PAGenes as a function of alkylation. (a) XRD, (b) FT-IR spectra, (c) TGA (the dash line is the derivative TGA of G-C_{12}_1), and (d) Raman spectra of pristine graphite and the as-prepared PAGenes after different reaction cycles. The diffraction peaks with star mark in part a may be attributed to less defined stage structures. For Raman spectra, the laser line is 532 nm.

by eight cycles of alkylation of graphite (G-C_{12}_8) along with the same amount of the starting material. The product shows a notable increase in volume. The covalently attached dodecyl functional groups render the exfoliated graphene sheets soluble in chloroform and other common organic solvents. Concentrated dispersions were readily obtained by bath sonication, with very little sediment even after two months (Figure 1b). When dodecyl functional groups were replaced by $-(CH_2)_5COOCH_3$ or $-(CH_2)_nCOOH$ (n = 5, 10) in the reductive alkylation, stable dispersions in *N*-methyl-pyrrolidone (NMP) or water were achieved (Supporting Information Figure S1). The readily soluble PAGenes are in stark contrast to graphene and pristine graphite, which have negligible solubility in common solvents.

More than 50% of the exfoliated graphene sheets have lateral sizes larger than 4 μm (Figure 1c). TEM provides further microscopic evidence for the structural integrity of the PAGenes (Figure 1d). Most of the fully exfoliated graphene sheets are uniformly transparent and stable under the electron beam. Electron diffraction (ED) pattern of the PAGenes (inset of Figure 1d) displays hexagonal symmetry similar to that of mechanically exfoliated graphene, confirming a well-crystallized, single- or bilayer graphene structure. Consistently, tapping-mode AFM imaging of PAGenes deposited on mica substrates shows a topographic height of ~0.5−0.7 nm (Figure 1e,f). The PAGenes exhibit an irregular shape with a size up to several micrometers in AFM, which is consistent with SEM observation. All the experimental evidence consistently suggests that by this simple reductive alkylation we have effectively exfoliated graphite into monolayer or few-layer graphene sheets.

2. Structural Evolution of PAGenes. To better understand and further optimize propagative alkylation of graphene, we followed the structural evolution of PAGenes for up to 8 reaction cycles with multiple characterization techniques including SEM, XRD, and Raman spectroscopy. The SEM images obtained from pristine graphite are shown in Supporting Information Figure S2a, where the graphite flakes are stacked to form compact structures in sizes of a few micrometers, with smooth faceted surface and sharp edges. However, after the first cycle of reductive alkylation, the graphite flakes show clear layered stacking morphology, in which the interlayer spacing of graphite was significantly increased. Moreover, as shown in Supporting Information Figure S2b, the edges of graphite flakes scrolled up, whereas the interiors remained flat. After the second (G-C_{12}_2) and eighth cycle (G-C_{12}_8) of alkylation (Supporting Information Figure S2c,d), the graphite flakes were exfoliated into very thin layers, exhibiting a crumpled morphology (Supporting Information Figure S2d). These results provide direct evidence for the exfoliation of graphite through progressive reductive alkylation.

XRD revealed further details of the alkylation induced exfoliation. As shown in Figure 2a, the XRD pattern of pristine graphite exhibits a characteristic (002) reflection peak at 2θ = 26.5°, which corresponds to an interlayer d-spacing of 0.34 nm. All the other peaks are attributed to other diffraction peaks associated with hexagonal graphite. Except two for unreacted graphite, the diffraction peaks in the XRD patterns of alkylated samples can be attributed to the multiphase composition

dx.doi.org/10.1021/cm402880v | *Chem. Mater.* 2013, 25, 4487−4496

produced by the inhomogeneous alkylation and the insertion of alkyl functional groups in graphite lattice. For graphite oxides, it is reported that the (002) peak exhibits a large shift from 26.5° (*d*-spacing of 0.34 nm) to 10.5° (*d*-spacing of 0.83 nm) due to a lattice expansion by partial exfoliation.[26] However, after propagative alkylation the primary peak was found in the range 23.7−22.8°, corresponding to the interlayer *d*-spacing of 0.38−0.39 nm. These results indicated that a new graphite-like phase (phase A) formed in the alkylated samples such as G-C_{12}_1 which maintains the stacking structure of graphite without much lattice expansion. Since the alkylation reaction propagated from graphite edges, the initial exfoliation of phase A in the solid state can be explained by edge-expansion. With increasing reaction cycle, the diffraction intensity decreased considerably with an obvious peak broadening over the range 18−30°. This diffraction evolution can be explained by the size reduction and lower crystallinity of phase A caused by propagative alkylation on graphene lattice. In addition, the initial exfoliation induced by edge-expansion facilitated the introduction of alkyl functional groups into the host materials, leading to the formation of graphite intercalation compounds (GICs) which were indicated as phase B. The diffraction peaks associated with the GICs can be indexed using the identity period I_c, which is 1.18 nm for G-C_{12}_8. However, probably due to the low crystallinity induced by propagative alkylation, only weak and broad diffraction peaks with low indices of phase B such as (001) and (002) were detected in the XRD pattern. Since no Br impurities were detected in the elemental analysis of alkylated samples (Supporting Information Figure S3), the diffraction peaks in XRD pattern with star mark may be attributed to less defined stage structures.

FT-IR spectra of GCICs (Figure 2b) clearly show the alkyl C−H stretching (2800−3000 cm^{-1}) and deformation (1380−1470 cm^{-1}) modes, unambiguously confirming the rise of alkyl peaks after the functionalization. At increasing reaction cycles, the C—H stretching modes grew with respect to the C═C stretching vibration in graphene (1584 cm^{-1}). The degree of functionalization was quantified by thermogravimetric analysis. As shown in Figure 2c, the pristine graphite materials exhibit negligible weight loss up to 700 °C, whereas the total weight loss of alkylated graphene sheets after one cycle of reductive alkylation is approximately 33%, occurring at 210 °C (∼12%) and 498 °C (∼21%), respectively. The first peak was attributed to the desorption of water or solvents in products, while the other peak was mainly caused by the thermal decomposition of dodecyl functional groups in graphene layers at elevated temperatures. Correspondingly, 1.9% of the graphene carbon atoms were covalently attached with alkyl functional groups after one cycle of alkylation. As reaction cycle increases, the weight loss increased monotonically up to 50% for the five-cycle products, corresponding to a functional degree of 2.8%. Consistently, Raman spectra of the exfoliated graphene sheets show high degrees of functionalization at increasing reaction cycles. For pristine graphite the Raman spectrum shows a weak D-band at 1352 cm^{-1} associated with the edge and the randomly distributed initial defects. The two most intense peaks are the G peak at 1580 cm^{-1} and the broad and asymmetric 2D peak at ∼2650−2750 cm^{-1}. The ratio of the D band to G peak intensity (I_D/I_G) is 0.19. After the first cycle of reaction (red line), a strong D-band appears at 1340 cm^{-1} (Figure 2d). The large I_D/I_G ratio (1.26) indicates the efficient functionalization on graphene layers. After the second cycle of reaction, the relative intensity of D-band further increased to yield a I_D/I_G ratio as high as 1.98. We found that the relative intensity of the Raman D-band increased monotonically up to the eight cycle of reaction investigated here. This trend reflects a progressive increase of sp^3 defects in the graphene lattice.

Figure 2d also shows significant changes in shape and relative intensity of the 2D peaks of the exfoliated graphene sheets compared to pristine graphite. The broad and asymmetric 2D peak of graphite at ∼2650−2750 cm^{-1} consists of two component peaks, $2D_1$ at lower frequency and $2D_2$ at higher frequency, respectively.[27,28] After the first cycle of alkylation, the 2D peak shifts to a lower frequency at ∼2675 cm^{-1}, exhibiting a sharp and more symmetric line shape. It is known that the 2D peak can be used to determine the specific number of stacked graphene layers.[29] For monolayer graphene, the 2D peak exhibits a single and sharp Lorentzian-like line at ∼2700 cm^{-1}. With increasing number of layers such as a bilayer, the 2D peak has a broader and up-shifted line shape, typically containing four components. For graphene sheets containing more than 5 layers, the Raman spectrum is undistinguishable from that of graphite. By comparison with those in the literature,[29,30] the exfoliated sheets obtained after one cycle of alkylation were categorized as few-layer (<5) graphene. At increasing alkylation cycles, the corresponding full width at half-maximum (fwhm) of the 2D peak slightly increased, which is consistent with the increase of defects in graphene.[18]

The structural evolution of the exfoliated graphene sheets suggests a propagative nature of the reductive alkylation. In the presence of naphthalene, graphite was reduced at room temperature in THF solution by lithium (Scheme 1).[31] This reaction is analogous to the Billups−Birch reduction where solvated electrons in liquid ammonia reduce CNTs leading to their effective exfoliation.[16,17] In THF, naphthalene can take up the electrons of alkali metals, resulting in the formation of alkali metal−THF complex ions and naphthalene anion radicals. As charge transfer occurs from naphthalene anion to the graphite, the alkali metal−THF complex ions are intercalated into the graphite lattice. Thus, the graphite layers are effectively separated by alkali metal−THF complex ions, and the $\pi-\pi$ interactions between them are replaced by electrostatic interactions, resulting in weakened interactions and increased spacing between adjacent graphitic layers. XRD patterns confirm that the majority of graphite can react with Li to form GICs.[32]

Alkyl radicals produced *in situ* by addition of alkyl halide covalently functionalized the exfoliating graphene sheets. We have previously reported that the Billups−Birch alkylation occurs by defect activation and propagates exclusively from defect sites.[20] Here we found that the alkylation of graphene preferably occurred from its edges. The alkylation converts the modified carbon from sp^2 hybridization to sp^3. The introduced sp^3 defects can act as new defect centers for continued propagation of the reaction fronts, resulting in the progressive alkylation of graphene layer from edge to the interior. The steric demand associated with the covalent alkylation of the graphene lattice further increases the interlayer spacing thus preventing the $\pi-\pi$ interaction and leading to the observed efficient exfoliation of graphene sheets. The increased interlayer spacing in GICs presumably facilitated the alkylation of graphene layers, while the attachment of alkyl functional groups sterically exfoliated graphene layers. Since the alkylation preferably occurred from the edges, it is not surprising that the edges of graphite exfoliated to form a scrolling structure. As the reaction fronts propagated from edge to interior, the graphite

dx.doi.org/10.1021/cm402880v | *Chem. Mater.* 2013, 25, 4487−4496

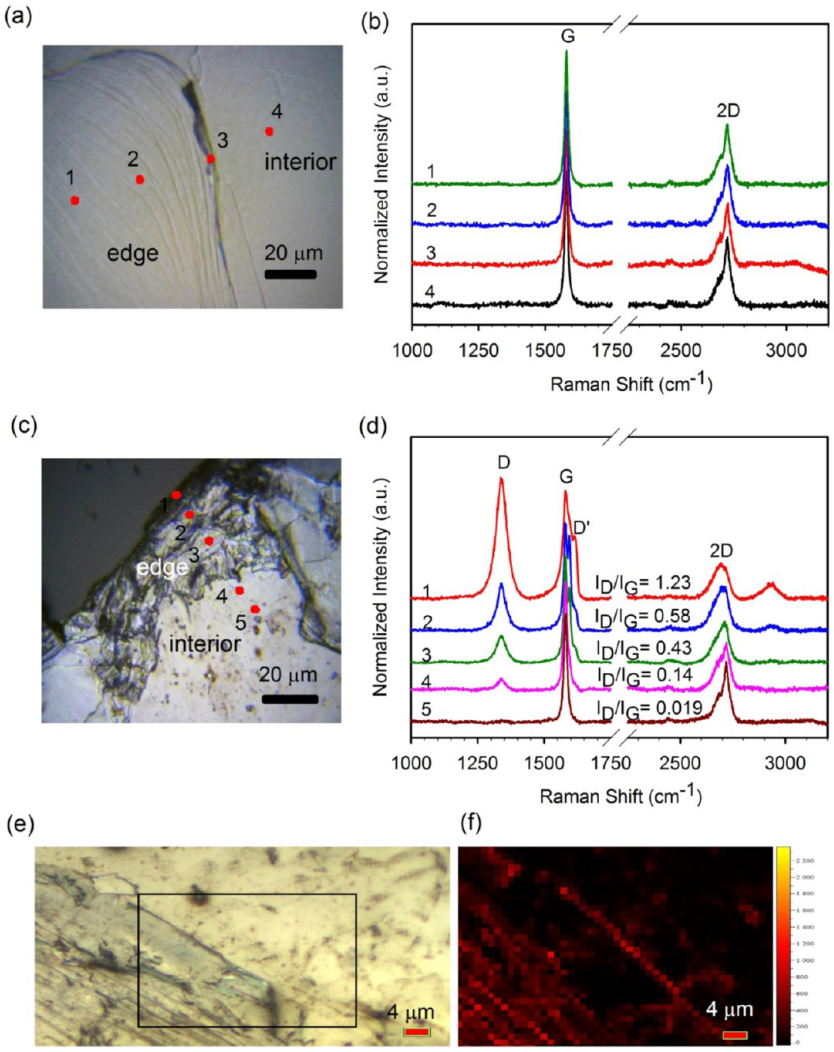

Figure 3. Spatially resolved spot Raman spectroscopy of HOPG flakes before (a, b) and after (c, d) one cycle of reductive alkylation. (f) Raman mapping of the D-band (1246−1413 cm^{-1}, step size = 1 μm, 100× objective) of the region indicated by the black box in part e.

was readily exfoliated to thinner flakes. Although alkylation of graphite is demonstrated in a recent experiment,[33] the propagative chemistry here makes it possible to efficiently exfoliate high quality graphene sheets.

To gain further insight into this propagation induced exfoliation mechanism, HOPG flakes obtained by micromechanical exfoliation[34] were chosen as a high quality graphite source and used as a better defined model system. One cycle of reductive alkylation was performed under similar conditions, using 1-bromododecane as the alkyl halide source. Figure 3 shows the photographs and Raman spectra of HOPG flakes before and after reaction. The pristine HOPG flake exhibits a smooth surface, where the edge steps caused by mechanical exfoliation are visible (Figure 3a). We followed the HOPG flake from the edge to the interior with spatially resolved spot Raman spectroscopy. As shown in Figure 3b, all the spectra display two identical Raman features in the range 1000−3250 cm^{-1}: the G peak at ∼1578 cm^{-1} corresponds to E_{2g}-symmetry phonons at the Brillouim zone center of sp^2-bonded carbon atoms, and the 2D peak at ∼2717 cm^{-1} originates from a second-order two-phonon process.[35] However, after alkylation, the surface of HOPG flake exhibits considerable changes: the edges scrolled to form a crumpled morphology (Figure 3c), and the steps are no longer distinguishable. Correspondingly, the edges show significantly larger Raman D-bands than those of the interiors (Figure 3d). At the edge of the HOPG flakes such as point 1 in Figure 3c, the spectrum shows a strong D-band around 1337 cm^{-1} with I_D/I_G = 1.23, in comparison with negligible D-band in the pristine HOPG. The intensities of the D-band monotonically decrease toward the central region of the flake. In the interior area, e.g., point 5 in Figure 3c, the obtained Raman spectrum shows negligible D and D′ bands, which is spectrally identical with that of pristine HOPG flakes. These trends suggest that the interiors of the flake remain intact during the alkylation reactions. Figure 3d also shows obvious changes in the shape and position of the 2D peak of the edges compared to the pristine HOPG. The 2D peak of pristine HOPG at ∼2717 cm^{-1} can be fitted into two Lorentzian-like peaks due to its AB stacking character.[35] However, the 2D peak of the edge points such as point 1 shifts to ∼2694 cm^{-1} and appears much more symmetric, supporting the presence of few-layer graphene. These observations support the proposed propagation and exfoliation mechanism of graphene layers, where reaction propagates inward from the edges of HOPG flakes, exfoliating graphene layers presumably due to the steric demand of the large functional groups.

Further evidence of propagative alkylation from the HOPG edges is given by Raman mapping of the D-band intensity. As

dx.doi.org/10.1021/cm402880v | *Chem. Mater.* 2013, 25, 4487−4496

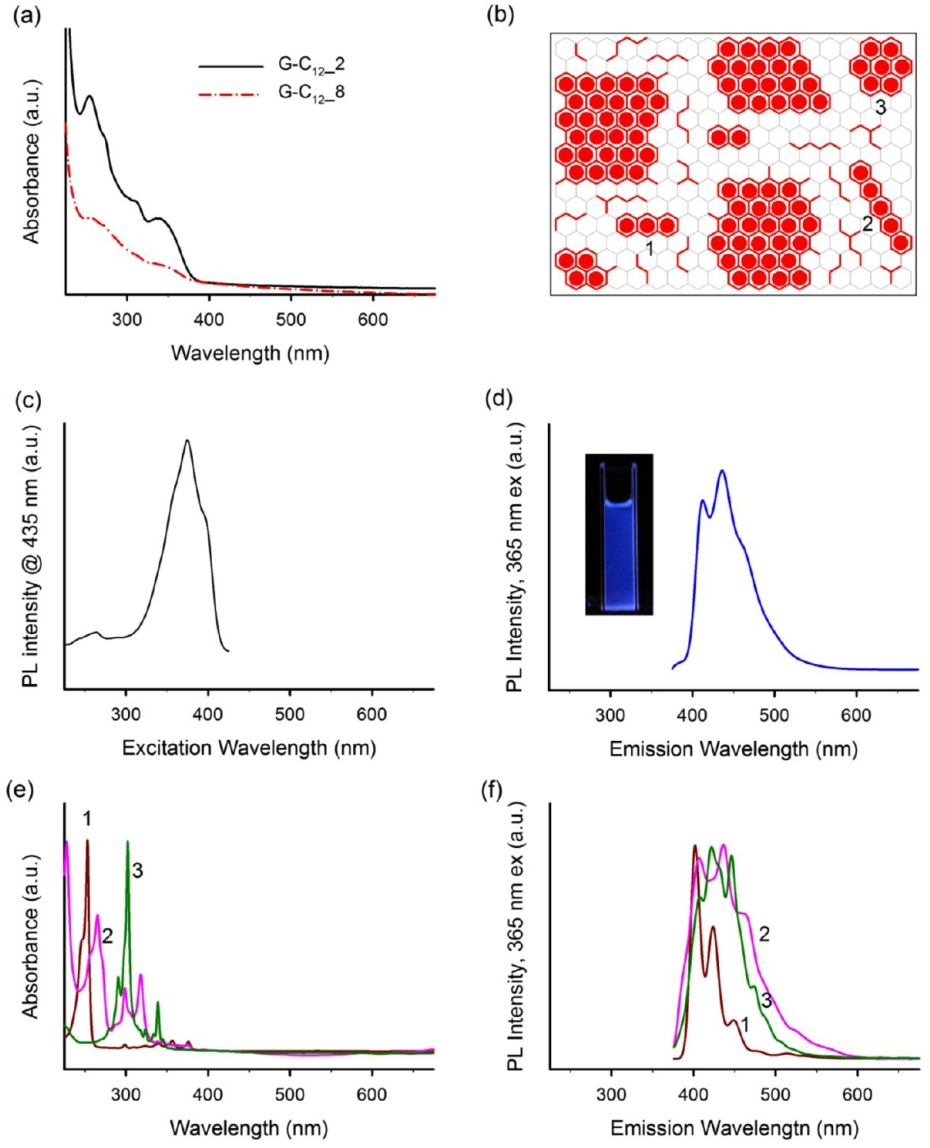

Figure 4. On-graphene molecular fragments. (a) UV−vis absorption spectra of PAGenes in ethanol. (b) A molecular model of "islanded" graphene structure, where red and gray color are intact (sp^2 hybridized) and functionalized (sp^3 hybridized) carbon atoms, respectively. For clarity, the functional groups are omitted. (c) Excitation spectrum with the detection wavelength of 435 nm and (d) PL spectra of PAGenes (G-C_{12}_2). Inset is a photograph of the PAGenes under 365 nm irradiation. (e) and (f) Absorption and photoluminescence spectra of small π-conjugated molecular systems corresponding to the fragments labeled in part (b), respectively.

shown in Figure 3f, upon alkylation, the D-band developed more strongly at the edges of the HOPG flake, signaling the preferential introduction of sp^3 defects by reaction propagation from the edges. When 1-bromododecane was replaced by 6-bromohexanoic acid, 11-bromoundecanoic acid, and methyl 6-bromohexanoate in reductive alkylation of graphite, we found similar trends of reaction propagation and exfoliated, crumpled few-layer graphene (Supporting Information Figures S4−S6). When acids and esters were used in the reductive alkylation, side reactions such as the generation of H_2 and the partial reduction of carboxyl group were also observed (Supporting Information Figure S5).

3.3. Optical Properties of PAGenes. PAGenes show interesting optical properties unattainable in graphene, as revealed by absorption and fluorescence spectroscopy. Shown in Figure 4a (black line) is the absorption spectrum of dodecylated PAGenes after the second cycle of reaction (G-C_{12}_2). The strong absorbance in the range 200−230 nm can be attributed to the $\pi-\pi^*$ transitions of C═C bonds in graphitic structures. A series of much weaker bands in the range 240−400 nm, exemplified by 254, 272, 310, and 340 nm, were also observed. When excited with UV light, the dodecylated PAGenes emits bright blue photoluminescence. The inset in Figure 4d shows a photograph of the dispersed PAGenes (G-C_{12}_2) excited by 365 nm light. The blue emission was strong enough to be easily seen by the naked eye. As shown in Figure 4d, the PAGenes show multiple emission peaks in the range 400−500 nm. In particular, with 365 nm excitation, the alkylated graphene sheets exhibit clear features at 410 and 435 nm, together with a small shoulder at 455 nm. The PL quantum yield, measured using Rhodamine B as a reference, is 12.5%. We note that graphene is a semimetal without a band gap. Opening a band gap in graphene is crucial for its potential applications in electronics. The observed photoluminescence

dx.doi.org/10.1021/cm402880v | *Chem. Mater.* 2013, 25, 4487−4496

suggests that propagative alkylation may provide an avenue to chemically opening a band gap in graphene.

We propose a molecular model of PAGenes (Figure 4b), in which intact (sp^2 hybridized) and functionalized (sp^3 hybridized) regions interlace. Within the same graphene lattice, smaller sp^2 clusters such as few aromatic rings or other sp^2 conjugates are dispersed in a sp^3 matrix, where a large fraction of carbons are bonded with dodecyl functional groups. This model is supported by comparative spectral analysis of PAGenes with small π-conjugated molecular systems such as anthracene, pentacene, and coronene (Figure 4e,f). The striking similarity in both the absorption and fluorescence spectra suggests that the spectral features observed in PAGenes arises from on-graphene small sp^2 domains generally resembling conjugated molecular systems[36,37] and graphene quantum dots.[38,39]

This spectral analysis provides evidence that propagative alkylation leads to the development of interesting patterns of small π-conjugation systems on graphene. After heavy functionalization, the extended π-conjugated network is broken into small π-conjugated systems embedded within the graphene lattice. These observations consistently support the theory that the propagative alkylation mechanism observed in SWCNTs similarly occurs in graphene.[20] Through reaction propagation that starts at edge defects or defects initially present in graphene structure, the large sp^2 domain in graphene layer is gradually broken into small conjugated systems separated by sp^3 hybridized carbon. As propagation occurs, the fraction of sp^3 regions is expected to increase until the smaller sp^2 clusters ultimately disappear. The highly functionalized PAGenes, G-C_{12}_8 (red line in Figure 4a), indeed exhibited much weaker absorbance in the range 240−400 nm than that of the less functionalized graphene sheets, G-C_{12}_2. The observed decrease in the absorption intensity can be attributed to the decreased concentration of small sp^2 domains. This model is consistent with Raman results. As shown in Figure 2d, the two new features at ∼1123 and 1511 cm^{-1} observed in the Raman spectrum of G-C_{12}_2 can be assigned to the C—C and C═C stretching vibrations of small sp^2 domains, which has been reported in the literature.[18,40] A similar phenomenon was observed in heavily functionalized SWCNTs by propagative sidewall alkylation (Supporting Information Figure S7), suggesting that the propagative nature of reductive alkylation is universal with sp^2 carbon systems.

We note that the oxidative reactions of graphite are known to occur preferentially from defects and edges. However, oxidation tends to remove carbon atoms from the graphene lattice, which is in stark contrast with the propagative alkylation reported here. The alkylation covalently attached the functional groups to the graphene lattice, without removing carbon from the lattice. Furthermore, the chemical structure of oxidized graphite varies with the degree of oxidation. On thte basis of various characterization techniques, many structural models have been proposed to unravel the chemical structure of GOs derived from the exfoliation of oxidized graphite.[41] In addition to the random distribution of oxygen-containing functional groups such as epoxides, carboxyl, and hydroxyl groups, the produced GOs were found to contain considerable irreversible structural defects as a result of the removal of carbon atoms from the graphene lattice during oxidation. Furthermore, although GOs contain isolated aromatic domains,[42] the emission efficiency of GOs is low.[43] This low emission efficiency may be explained by the nonradiative recombination of localized electron−hole pairs induced by epoxy and carboxylic groups. By passivation of surface reactive sites or control of the reduction chemistry of GOs, the emissive properties of GOs can be improved.[44,45] However, the mechanistic details are more complex, and the fluorescence is not as bright as observed in the system reported here.

3.4. Electrical Percolation in PAGenes Films. Theoretical and experimental studies have shown that the pattern of functional groups on sp^2 carbon lattices such as SWCNTs will substantially affect their electrical and optical properties.[46−49] For example, a defect density of ∼1/10 000 is sufficient to completely quench exciton photoluminescence of SWCNTs.[49] However, by propagative alkylation, the functional groups were confined along the tubular direction, resulting in alternating bands of functionalized and intact regions through reaction propagation that starts at initial defects.[20] The covalently functionalized SWCNTs not only exhibit high water solubility but also retain some of the optical properties of pristine SWCNTs[20] and induce a red-shift of the near-infrared photoluminescence.[25] When the propagative alkylation was applied to graphite, full exfoliation of graphene layers was achieved. The obtained PAGenes exhibit high solubility in organic solvents or water as shown above, making this material superior to mechanically exfoliated or CVD grown graphene in applications where scalability and solution processing are desirable. However, does the ability to covalently functionalize graphene disrupt its electronic structure as observed in GOs?

In order to investigate the electrical properties, we measured the room temperature electrical conductivities of compressed-powder samples of PAGenes and GOs, respectively, using a four probe method. For PAGenes after the first cycle of alkylation (G-C_{12}_1), the electrical conductivity was as high as 4.1×10^3 S/m. After the second cycle of alkylation, the conductivity decreased to 1.7×10^3 S/m. The decrease can be explained by the gradual removal of large sp^2 domains as the propagative alkylation occurs. However, the electrical conductivity of G-C_{12}_2 is still 5 orders of magnitude greater than those of GOs (3.3×10^{-2} S/m).

However, if PAGenes were covalently functionalized by alkyl groups, which convert the modified carbon atoms from sp^2 hybridization to sp^3, how could PAGenes have retained their electrical properties so well? We attribute the observed high electrical conductivity to efficient electrical percolation in PAGenes. As shown in Figure 4b, the "islanded" structure of dodecylated graphene contains sp^2 and sp^3 hybridized carbon clusters, corresponding to intact and functionalized regions. The electrical contact of the intact regions between different layers could provide a continuous conductive pathway in the graphene film (Figure 5). This mechanism is consistent with what we observed in covalently functionalized carbon nanotubes with banding functionalization,[50] suggesting a powerful general approach to improve thin film conductivity in carbon nanomaterials by controlling functionalization patterns on the carbon lattices. It is also important to note that the covalently attached alkyl functional groups can be thermally removed. Upon thermal treatment, the typical graphitic XRD diffraction pattern is recovered (Supporting Information Figure S8). The electrical conductivity of the thermal-treated PAGenes increased to 1.1×10^4 S/m, which is comparable with that of graphite (1.8×10^4 S/m), confirming the reversibility of the alkylation chemistry.

dx.doi.org/10.1021/cm402880v | Chem. Mater. 2013, 25, 4487−4496

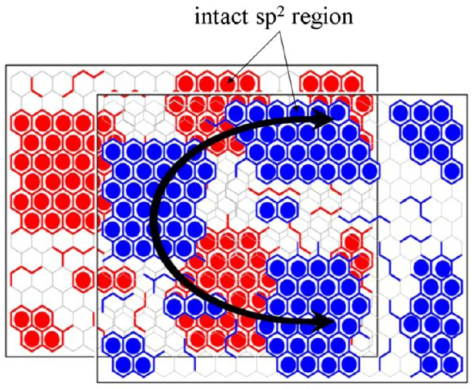

Figure 5. Schematic of electrical percolation of PAGenes through intact sp^2 regions.

CONCLUSIONS

Propagative alkylation efficiently exfoliated graphite and covalently functionalized graphene sheets. The propagative functionalization expands the interlayer spacing of graphite, making their direct exfoliation possible. The exfoliated, alkylated graphene sheets are soluble in common solvents such as chloroform, water, and NMP, depending on the functional groups. The propagation and exfoliation of graphene layers were confirmed by SEM, TEM, AFM, and Raman spectroscopy. Since the reductive alkylation occurs on graphene structure by defect activation and propagates from sp^3 defect sites, the controlled functionalization gives rise to an "islanded" graphene structure containing intact and functionalized regions, with smaller sp^2 domains interlaced with sp^3 regions. The PAGenes films show high electrical conductivity, which can be attributed to electrical percolation via contacts of the intact sp^2 regions.

ASSOCIATED CONTENT

Supporting Information

Photographs of graphite and PAGenes dispersions in NMP and water, SEM images of pristine graphite and dodecylated products at different stages of reaction, elemental analysis of dodecylated sample, XRD patterns, IR spectra, Raman spectra, and SEM images of PAGenes with different functional groups, Raman spectra of propagatively functionalized SWCNTs with different functional groups, and XRD pattern of thermally defunctionalized PAGenes. This material is available free of charge via the Internet at http://pubs.acs.org.

AUTHOR INFORMATION

Corresponding Authors

*E-mail: sldeng@xmu.edu.cn.
*E-mail: yhw@umd.edu.

Notes

The authors declare no competing financial interest.

ACKNOWLEDGMENTS

This work was partially supported by the National Key Basic Research Program of China (2013CB933901), the National Natural Science Foundation of China (No. 21171140, 21021061, 21031004, U1205111), the Natural Science Foundation of Fujian Province of China (No. 2013J01056), and the Fundamental Research Funds for the Central Universities. Y.H.W. acknowledges support from the University of Maryland and the U.S. National Science Foundation (CAREER CHE-1055514). We thank Bin Ren and Chuan-Jing Huang for access to the Raman microscopes, Jia-Wei Yan for access to the AFM instrument, and Mr. Yi-Liang Zhu and Mr. Jun-Yang Liu for assistance with electrical conductivity measurement.

REFERENCES

(1) Geim, A. K.; Novoselov, K. S. *Nat. Mater.* **2007**, *6*, 183.
(2) Novoselov, K. S.; Geim, A. K.; Morozov, S. V.; Jiang, D.; Zhang, Y.; Dubonos, S. V.; Grigorieva, I. V.; Firsov, A. A. *Science* **2004**, *306*, 666.
(3) Berger, C.; Song, Z.; Li, X.; Wu, X.; Brown, N.; Naud, C.; Mayou, D.; Li, T.; Hass, J.; Marchenkov, A. N.; Conrad, E. H.; First, P. N.; de Heer, W. A. *Science* **2006**, *312*, 1191.
(4) Li, X.; Cai, W.; An, J.; Kim, S.; Nah, J.; Yang, D.; Piner, R.; Velamakanni, A.; Jung, I.; Tutuc, E.; Banerjee, S. K.; Colombo, L.; Ruoff, R. S. *Science* **2009**, *324*, 1312.
(5) Kim, K. S.; Zhao, Y.; Jang, H.; Lee, S. Y.; Kim, J. M.; Kim, K. S.; Ahn, J.-H.; Kim, P.; Choi, J.-Y.; Hong, B. H. *Nature* **2009**, *457*, 706.
(6) Reina, A.; Jia, X.; Ho, J.; Nezich, D.; Son, H.; Bulovic, V.; Dresselhaus, M. S.; Kong, J. *Nano Lett.* **2009**, *9*, 30.
(7) Wu, Q.; Xu, Y.; Yao, Z.; Liu, A.; Shi, G. *ACS Nano* **2010**, *4*, 1963.
(8) Fowler, J. D.; Allen, M. J.; Tung, V. C.; Yang, Y.; Kaner, R. B.; Weiller, B. H. *ACS Nano* **2009**, *3*, 301.
(9) Qu, L.; Liu, Y.; Baek, J.-B.; Dai, L. *ACS Nano* **2010**, *4*, 1321.
(10) Machado, B. F.; Serp, P. *Catal. Sci. Technol.* **2012**, *2*, 54.
(11) Park, S.; Ruoff, R. S. *Nat. Nanotechnol.* **2009**, *4*, 217.
(12) Chen, D.; Feng, H.; Li, J. *Chem. Rev.* **2012**, *112*, 6027.
(13) Hummers, W. S., Jr.; Offeman, R. E. *J. Am. Chem. Soc.* **1958**, *80*, 1339.
(14) Cai, W.; Piner, R. D.; Stadermann, F. J.; Park, S.; Shaibat, M. A.; Ishii, Y.; Yang, D.; Velamakanni, A.; An, S. J.; Stoller, M.; An, J.; Chen, D.; Ruoff, R. S. *Science* **2008**, *321*, 1815.
(15) Coleman, J. N. *Acc. Chem. Res.* **2013**, *46*, 14.
(16) Liang, F.; Sadana, A. K.; Peera, A.; Chattopadhyay, J.; Gu, Z.; Hauge, R. H.; Billups, W. E. *Nano Lett.* **2004**, *4*, 1257.
(17) Liang, F.; Alemany, L. B.; Beach, J. M.; Billups, W. E. *J. Am. Chem. Soc.* **2005**, *127*, 13941.
(18) Englert, J. M.; Dotzer, C.; Yang, G.; Schmid, M.; Papp, C.; Gottfried, J. M.; Steinruck, H.-P.; Spiecker, E.; Hauke, F.; Hirsch, A. *Nat. Chem.* **2011**, *3*, 279.
(19) Zhong, Y. L.; Swager, T. M. *J. Am. Chem. Soc.* **2012**, *134*, 17896.
(20) Deng, S.; Zhang, Y.; Brozena, A. H.; Mayes Maricris, L.; Banerjee, P.; Chiou, W.-A.; Rubloff, G. W.; Schatz, G. C.; Wang, Y. *Nat. Commun.* **2011**, *2*, 382.
(21) Deng, S. L.; Brozen, A. H.; Zhang, Y.; Piao, Y. M.; Wang, Y. H. *Chem. Commun.* **2011**, *47*, 758.
(22) Deng, S.; Piao, Y.; Brozena, A. H.; Wang, Y. H. *J. Mater. Chem.* **2011**, *21*, 18568.
(23) Sun, C.-F.; Karki, K.; Jia, Z.; Liao, H.; Zhang, Y.; Li, T.; Qi, Y.; Cumings, J.; Rubloff, G. W.; Wang, Y. *ACS Nano* **2013**, *7*, 2717.
(24) Zhang, Y.; Wang, Y. H. *J. Phys. Chem. Lett.* **2011**, *2*, 885.
(25) Zhang, Y.; Valley, N.; Brozena, A. H.; Piao, Y.; Song, X.; Schatz, G. C.; Wang, Y. H. *J. Phys. Chem. Lett.* **2013**, *4*, 826.
(26) Dikin, D. A.; Stankovich, S.; Zimney, E. J.; Piner, R. D.; Dommett, G. H. B.; Evmenenko, G.; Nguyen, S. T.; Ruoff, R. S. *Nature* **2007**, *448*, 457.
(27) Vidano, R. P.; Fischbach, D. B.; Willis, L. J.; Loehr, T. M. *Solid State Commun.* **1981**, *39*, 341.
(28) Nemanich, R. J.; Solin, S. A. *Phys. Rev. B: Condens. Matter Mater. Phys.* **1979**, *20*, 392.
(29) Ferrari, A. C.; Meyer, J. C.; Scardaci, V.; Casiraghi, C.; Lazzeri, M.; Mauri, F.; Piscanec, S.; Jiang, D.; Novoselov, K. S.; Roth, S.; Geim, A. K. *Phys. Rev. Lett.* **2006**, *97*, 187401/1.
(30) Shih, C.-J.; Vijayaraghavan, A.; Krishnan, R.; Sharma, R.; Han, J.-H.; Ham, M.-H.; Jin, Z.; Lin, S.; Paulus, G. L. C.; Reuel, N. F.; Wang, Q. H.; Blankschtein, D.; Strano, M. S. *Nat. Nanotechnol.* **2011**, *6*, 439.

(31) Nomine, M.; Bonnetain, L. *J. Chim. Phys. Phys.-Chim. Biol.* **1969**, *66*, 1731.
(32) Inagaki, M.; Tanaike, O. *Synth. Met.* **1995**, *73*, 77.
(33) Kelly, K. F.; Billups, W. E. *Acc. Chem. Res.* **2013**, *46*, 4.
(34) Novoselov, K. S.; Jiang, D.; Schedin, F.; Booth, T. J.; Khotkevich, V. V.; Morozov, S. V.; Geim, A. K. *Proc. Natl. Acad. Sci. U.S.A.* **2005**, *102*, 10451.
(35) Malard, L. M.; Pimenta, M. A.; Dresselhaus, G.; Dresselhaus, M. S. *Phys. Rep.* **2009**, *473*, 51.
(36) Payne, M. M.; Parkin, S. R.; Anthony, J. E. *J. Am. Chem. Soc.* **2005**, *127*, 8028.
(37) Boehme, T.; Simpson, C. D.; Muellen, K.; Rabe, J. P. *Chem.—Eur. J.* **2007**, *13*, 7349.
(38) Yan, X.; Cui, X.; Li, L.-s. *J. Am. Chem. Soc.* **2010**, *132*, 5944.
(39) Gupta, V.; Chaudhary, N.; Srivastava, R.; Sharma Gauri, D.; Bhardwaj, R.; Chand, S. *J. Am. Chem. Soc.* **2011**, *133*, 9960.
(40) Ferrari, A. C.; Robertson, J. *Phys. Rev. B: Condens. Matter Mater. Phys.* **2001**, *63*, 121405.
(41) Szabo, T.; Berkesi, O.; Forgo, P.; Josepovits, K.; Sanakis, Y.; Petridis, D.; Dekany, I. *Chem. Mater.* **2006**, *18*, 2740.
(42) Wilson, N. R.; Pandey, P. A.; Beanland, R.; Young, R. J.; Kinloch, I. A.; Gong, L.; Liu, Z.; Suenaga, K.; Rourke, J. P.; York, S. J.; Sloan, J. *ACS Nano* **2009**, *3*, 2547.
(43) Sun, X.; Liu, Z.; Welsher, K.; Robinson, J. T.; Goodwin, A.; Zaric, S.; Dai, H. *Nano Res.* **2008**, *1*, 203.
(44) Mei, Q.; Zhang, K.; Guan, G.; Liu, B.; Wang, S.; Zhang, Z. *Chem. Commun.* **2010**, *46*, 7319.
(45) Eda, G.; Lin, Y.-Y.; Mattevi, C.; Yamaguchi, H.; Chen, H.-A.; Chen, I. S.; Chen, C.-W.; Chhowalla, M. *Adv. Mater.* **2010**, *22*, 505.
(46) Garcia-Lastra, J. M.; Thygesen, K. S.; Strange, M.; Rubio, A. *Phys. Rev. Lett.* **2008**, *101*, 236806/1.
(47) Lopez-Bezanilla, A.; Triozon, F.; Latil, S.; Blase, X.; Roche, S. *Nano Lett.* **2009**, *9*, 940.
(48) Goldsmith, B. R.; Coroneus, J. G.; Khalap, V. R.; Kane, A. A.; Weiss, G. A.; Collins, P. G. *Science* **2007**, *315*, 77.
(49) Cognet, L.; Tsyboulski, D. A.; Rocha, J.-D. R.; Doyle, C. D.; Tour, J. M.; Weisman, R. B. *Science* **2007**, *316*, 1465.
(50) Brozena, A. H.; Moskowitz, J.; Shao, B. Y.; Deng, S. L.; Liao, H. W.; Gaskell, K. J.; Wang, Y. H. *J. Am. Chem. Soc.* **2010**, *132*, 3932.